Communication

Wideband and Miniaturized Phase-Corrected Empty Substrate-Integrated H-Plane Horn Antenna for 5G Millimeter Waves

Ningning Yan, Chuansheng Ji, Yu Luo, and Kaixue Ma

***Abstract*— This communication introduces a substrate-integrated H-plane horn antenna with phase-corrected structures. The quadratic curves etched on the horn aperture improve the impedance matching and the gain performance. The quasi-uniform phase distribution is achieved by the phase-corrected structure, which consists of the quadratic curves and metallized via-holes embedded symmetrically on the top and bottom layers. To integrate with other planar circuits and test the proposed antenna, the transition from microstrip line to empty substrate-integrated waveguide (ESIW) is used. Compared with the optimum horn, the proposed antenna realizes a 60% reduction of the longitudinal length. A wide impedance bandwidth of 22% for |S11| < −10 dB, which covers the n257, n258, and n261 5G frequency bands (24.25–29.5 GHz), is verified by a fabricated prototype. Moreover, the stable realized gain varying from 9.3 to 11 dBi is obtained during the operating bandwidth.**

***Index Terms*— 5G, empty substrate-integrated waveguide (ESIW), horn antenna, millimeter waves (mmWs), phase corrected.**

I. Introduction

With the rapid development of 5G wireless communication, millimeter-wave (mmW) antennas have driven more attention due to abundant frequency bands and the higher data transmission rate of mmW technologies [1]. The horn antenna has been widely used in communication systems owing to the advantages of simple structure, low cost, and high-power handling capacity [2]. Traditional metallic horn antennas are hard to be applied for the modern compact wireless platform because of the bulky volume, while the invention of substrate-integrated waveguide (SIW) H-plane horn antenna [3], [4] which has the merits of low profile, compact configuration, and ease of integration, solves this problem.

The substrate-integrated horn antenna usually suffers from poor bandwidth performance because of the impedance mismatch between the radiating aperture and air [5]. Several studies are reported to enhance the impedance matching and the gain performance of SIW H-plane antennas in recent years [6], [7], [9], [10], [11], [12], [13], [14], [15], [16]. Using the gap SIW technology to correct the phase distribution of the EM field across the horn aperture, the horn antenna in [6] achieves an enhanced gain of 10.3 dBi. By printing tapered-ladder transitions in front of the horn aperture, the horn antenna obtains an impedance bandwidth of 20%. The extended dielectric lens perforated with air vias of different diameters is adopted to play as a stepped impedance transformer to widen the bandwidth in [7], and the antenna obtains an operating bandwidth of 32%. Empty SIW (ESIW) can achieve low loss [8]. Mateo et al. [9] present an antenna adopting ESIW, which obtains a high efficiency about 90%, but the impedance bandwidth is narrow. In [10], an air-filled SIW (AFSIW) H-plane horn antenna is designed. The power divider and phase shifters inside AFSIW and a 1 × 4 planar dipole array enhance the aperture efficiency and antenna gain, which are 90% and 12.5 dBi, respectively. All horn antennas mentioned above need extended substrates to support performance-enhancement structures, which enlarges the dimensions of antennas.

The slow wave structures composed of metallized via-holes inside the flare region of the horn antenna in [11] realize a 53.83% reduction of longitudinal length and 1.1-dB improvement of gain on average compared with the optimum horn. However, the gain is still not high. Wang et al. [12] correct the phase distribution by adjusting the lengths and positions of three metal-via arrays, but the impedance bandwidth is narrow. Wang et al. [13] propose a three-layered substrate-integrated H-plane horn antenna with the dipole array loaded on top and bottom substrates. The dipole array as the complementary source of the horn antenna improves the impedance bandwidth and radiation properties, which realizes an impedance bandwidth of 40% and a stable gain from 9 to 12 dBi. This design needs extra fixing structures and cannot be integrated with planar circuits directly. The horn antenna in [14] realizes a bandwidth of 103% by cutting two air slots along the sides of the flare part of the antenna. Nevertheless, the antenna has a complex structure and is not easily integrated with planar circuits. Luo and Bornemann [15] introduce an SIW H-plane horn antenna with a pair of slots to suppress the back lobe, but the operating bandwidth is only 1.4%. The H-plane horn antenna in [16] realizes a high gain of 16 dBi; however, it suffers from bulky antenna size.

This communication proposes a novel miniaturized ESIW H-plane horn antenna composed of three substrates. By cutting quadratic curves on the metal layers of top and bottom substrates, the impedance matching and the gain have been improved, which are realized without additional structures in front of the horn aperture. The phase-corrected structure realizes a relatively uniform phase distribution of E-field by decreasing the equivalent permittivity of the region close to the edge of the horn antenna. Thus, the proposed antenna has a stable high gain performance. The metal-via holes inside the middle of top and bottom substrates reduce the residual E-fields inside top and bottom substrates, which further enhance the gain performance of the antenna. In addition, the longitudinal length of the proposed antenna is reduced by 60% compared with that of the optimum SIW horn, and the transition from microstrip line to ESIW makes the proposed antenna, which can be integrated with planar circuits easily. The measured results show that the horn antenna obtains an operating bandwidth from 24 to 30 GHz and a peak realized gain of 11 dBi.

Manuscript received 9 November 2022; revised 18 April 2023; accepted 1 June 2023. Date of publication 16 June 2023; date of current version 6 September 2023. This work was supported in part by the National Natural Science Foundation of China under Grant 62001324 and in part by the National Natural Science Foundation of China for Key Project under Grant 61831017. *(Corresponding author: Ningning Yan.)*

The authors are with the School of Microelectronics and the Tianjin Key Laboratory of Imaging and Sensing Microelectronic Technology, Tianjin University, Tianjin 300072, China (e-mail: ningning.yan@tju.edu.cn; j15212782058@163.com; yluo@tju.edu.cn; makaixue@tju.edu.cn).

Color versions of one or more figures in this communication are available at https://doi.org/10.1109/TAP.2023.3285354.

Digital Object Identifier 10.1109/TAP.2023.3285354

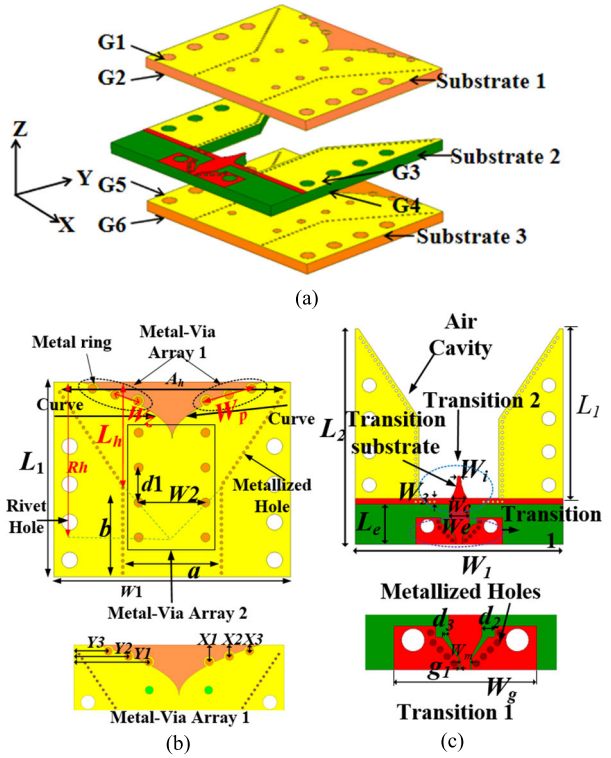

Fig. 1. Structure of the horn antenna. (a) 3-D view of the antenna. (b) Top view of substrates 1 and 3. (c) Top view of substrate 2.

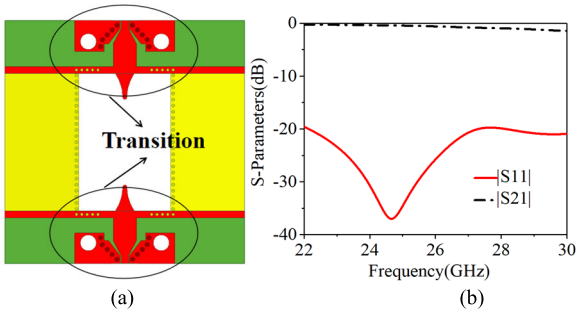

Fig. 2. (a) Back-to-back transition. (b) S-parameters of transition.

TABLE I
DIMENSIONS OF THE HORN ANTENNA (UNITS: mm)

Symbol	Quantity	Symbol	Quantity
L_1	25.7	Y_3	5.1
W_1	31.2	L_e	6
L_2	32.4	W_e	3
W_2	8.8	W_3	1
a	12	W_m	0.9
b	12	W_i	0.5
d_1	4.6	W_g	13
m	7.5	d_2	1.2
n	12	d_3	0.6
A_h	30.2	g_1	0.12
X_1	2.5	W_c	2.44
X_2	1.7	R_1	0.2
X_3	0.9	R_2	0.3
Y_1	11.1	Wp	7.4
Y_2	8.1	R_h	22.4
L_h	13.5	Wz	3.1

II. Antenna Design and Analysis

A. Antenna Configuration

As exhibited in Fig. 1(a), the proposed antenna is composed of three substrate layers named substrate 1, substrate 2, and substrate 3, respectively, and the middle substrate layer is sandwiched with the top and bottom grounded layers. Plated metal is on both sides of each substrate, and the corresponding six metal layers are named G1–G6. Fig. 1(b) shows the top view of substrates 1 and 3 in detail, which is the same as the bottom view. Substrate 1 that is exactly the same as substrate 3 is FR4 with an ε_{r1} of 4.4, a tan δ of 0.02, and a thickness of 1.5 mm. Four identical symmetrical curves etched on the plated metal layers G1, G2, G5, and G6 are introduced to improve the impedance matching between the radiating aperture and air. Six symmetrical metallized via-holes with a radius of 0.6 mm around the curves constitute Metal-Via Array 1, and there are extra metal rings around the six metallized holes considering the processing. W_Z is the distance between the centers of each via of Metal-Via Array 1.

The quadratic curves and the Metal-Via Array 1 of substrates 1 and 3 constitute the phase-corrected structure of the proposed horn antenna. The Metal-Via Array 2 composed of eight symmetrical metallized via-holes with a radius of 0.6 mm, which are embedded in the middle of the substrate, is used to reduce the capacitance between the metal layers on the both sides of the substrate. The distance between each metallized hole of Metal-Via Array 2 is adjusted to d_1, and the position of each metallized hole of Metal-Via Arrays 1 and 2 is exhibited in Fig. 1(b). As we can see from Fig. 1(c), the substrate material of Rogers 4003C with an ε_{r2} of 3.55, a tan δ of 0.0027, and a thickness of 1.524 mm is used for the substrate 2, which is cut to realize the air cavity. To support the feeding structure, substrate 2 has a length of L_2, which is longer than the length L_1 of substrates 1 and 3. Transition 1 from a 50-Ω grounded coplanar waveguide (GCPW) to a 50-Ω microstrip line is designed to connect to a test coaxial cable connector. Transition 2 from the microstrip line to ESIW contains a tapered substrate, which is illustrated in [8] in detail. The simulated S-parameters of the back-to-back transition are shown in Fig. 2(b), and it can be seen that the reflection coefficient is better than −19 dB and the insertion loss is better than 1.2 dB in the band from 22 to 30 GHz. All the designed parameters are given in Table I.

B. Design Analysis

Tapered structures are often used to improve the impedance matching of antennas [17], [18]. In order to obtain wider operating bandwidth, the tapered quadratic curves on the top and bottom substrates shown in Fig. 1(b) are introduced to etch out parts of the metal. The quadratic curves are designed according to the following equation:

$$y = ax^2 = \frac{m}{n^2}x^2. \tag{1}$$

As it is shown in Fig. 3, the origin coordinates point O is the intersection of two symmetrical quadratic curves, and the point P is at the edge of the G1 layer. The quadratic curve starts at point O (0, 0) and ends at point P (n, m), so a is equal to m/n^2 after being calculated.

To explain how the quadratic curves improve the matching between the radiating aperture and air, Ant 1 and Ant 2 exhibited in Fig. 4 are designed to do the comparison. The two antennas without the Metal-Via Arrays 1 and 2 have the same dimension. The curves of Ant 2 are etched on G1, G2, G5, and G6 layers, while Ant 1 has no curves. Simulated |S11| of Ants 1 and 2 in Fig. 4 is depicted in Fig. 5(a), respectively, and it can be seen that the impedance

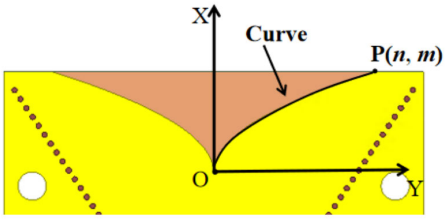

Fig. 3. Quadratic curve on G1 layer.

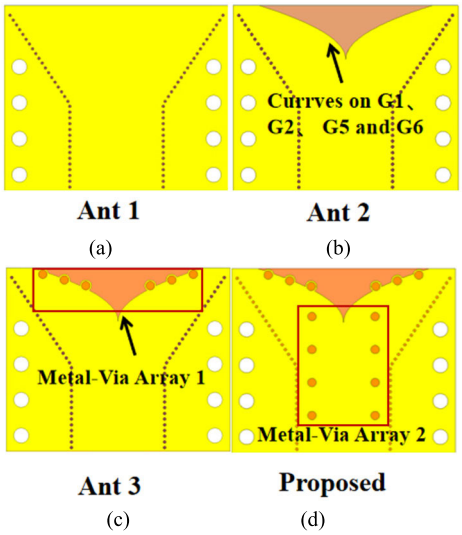

Fig. 4. Evolution of the horn antenna. (a) Ant 1. (b) Ant 2. (c) Ant 3. (d) Proposed.

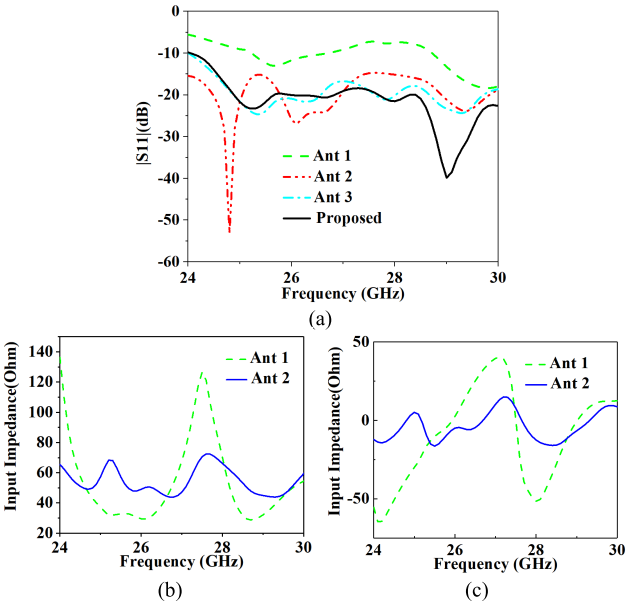

Fig. 5. Simulated |S11| and input impedances of Ants 1 and 2. (a) S-parameters. (b) Real part. (c) Imaginary part.

bandwidth becomes much wider after the curves are adopted. The impedance bandwidth for $|S11| < -10$ dB of Ant 2 covers the band from 24 to 30 GHz. Fig. 5(b) and (c) shows the input impedance of the two antennas, which can be seen that both the real and imaginary parts of the input impedance of Ant 1 show large fluctuation, which

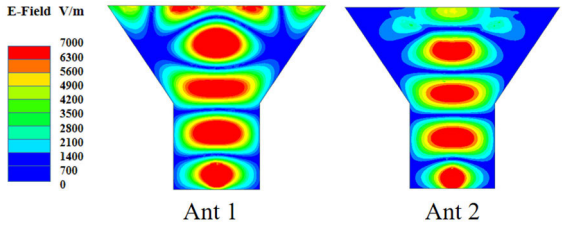

Fig. 6. Simulated E-field distributions in the air cavity of Ants 1 and 2 at 26.5 GHz.

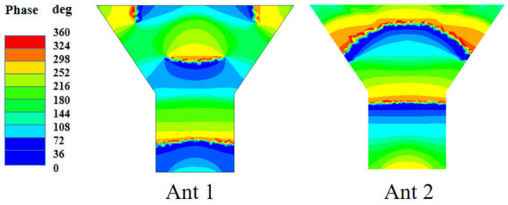

Fig. 7. Phase distributions of E-fields in the air cavity of Ants 1 and 2 at 26.5 GHz.

means the poor impedance matching between the radiating aperture and air [13].

For Ant 2, four curves etched on the metal layers of substrates 1 and 3 greatly decrease the fluctuation, and the real and imaginary parts of the input impedance of Ant 2 are close to 50 and 0 Ω, respectively. The reason is that the Q factor of the antenna descends after adding the curves. The middle parts of Ant 2 containing substrates and air have larger loss than the middle parts of Ant 1, which only contain air. As Fig. 6 shows, the electric field intensity in air cavity of Ant 1 is stronger than that of Ant 2, which means the Q factor of Ant 2 is smaller than that of Ant 1. According to formula (2), where f_0 is the resonance frequency, Ant 2 has a wider bandwidth BW than Ant 1. Thus, the impedance bandwidth of the proposed antenna is improved

$$\mathrm{BW} = f_0/Q. \tag{2}$$

Traditionally, the H-plane horn antenna should be designed according to formula (3) to obtain the optimum directivity by providing minimum phase error along the radiating aperture. As shown in Fig. 1(b), A_h is the dimension of the horn antenna at opening, R_h is the horn's radius, and L_h is the length of the horn antenna's flared region. The length L_h of the proposed antenna is reduced to 13.5 mm, which is shorted to 60% of the value calculated by formulas (3) and (4). However, reducing L_h will increase the phase difference Ψ between the center and the edge of the aperture according to formula (5) [2]; then, the gain will be decreased

$$A_h = \sqrt{3\lambda R} \tag{3}$$

$$L_h = R_h(1-a/A_h) \tag{4}$$

$$\Psi = \pi A_h(A_h - a)/4\lambda L_h. \tag{5}$$

The curves on the top and bottom substrates can also reduce the phase difference caused by the length reduction. It can be observed from Fig. 7 that the E-field in the air cavity of Ant 2 has a more uniform phase distribution compared with that of Ant 1. After etching curves, the equal permittivity ε_{r4} of the middle parts of Ant 2 containing substrates and air is bigger than the equal permittivity ε_{r3} of the middle parts of Ant 1, which only contain air. The phase velocity v_p is inversely proportional to the equivalent permittivity ε_{reff} for a fixed equivalent permeability μ_r as follows:

$$v_p = c/\sqrt{u_r \varepsilon_r} \tag{6}$$

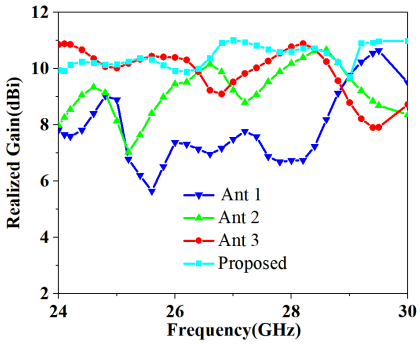

Fig. 8. Realized gain of Ant 1, Ant 2, Ant 3, and proposed antenna.

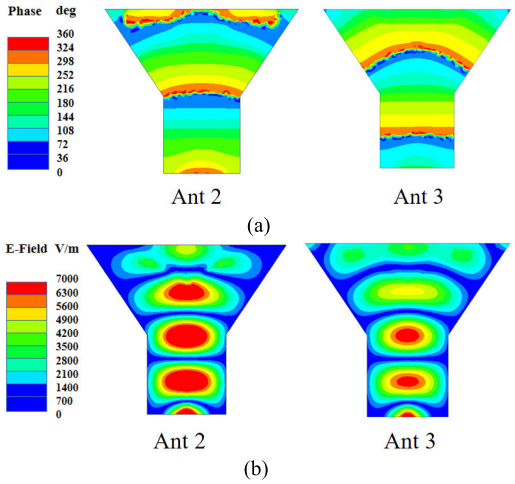

Fig. 9. Phase and magnitude distributions of E-field in the air cavities at 25 GHz. (a) Phase of Ants 2 and 3. (b) Magnitude of Ants 2 and 3.

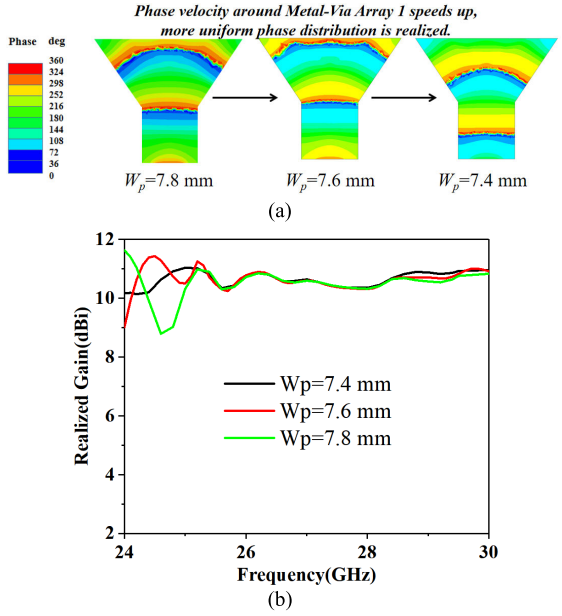

Fig. 10. Effect of parameter W_p on the phase distribution of E-field at 25 GHz and gain property. (a) Phase. (b) Realized gain.

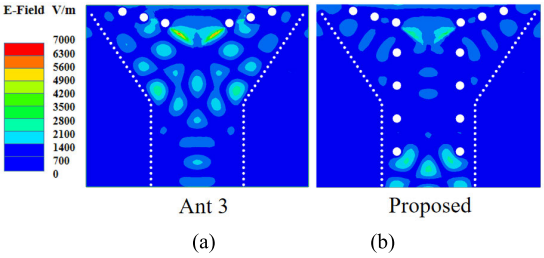

Fig. 11. Simulated E-field distributions inside the top substrates of Ant 3 and the proposed antenna at 27 GHz. (a) Ant 3. (b) Proposed antenna.

where c is the velocity of light in vacuum. Thus, the phase velocity in the middle of Ant 2 slows down and a relative uniform phase distribution is obtained, and the gain of Ant 2 is improved obviously than Ant 1. The average gain of Ant 2 is 9.2 dBi, while the average gain of Ant 1 is 7.8 dBi, which can be seen in Fig. 8.

However, the phase distribution of Ant 2 is not uniform enough. To further correct the phase difference caused by the length reduction, the phase-corrected structure, Metal-Via Array 1, is used, which is shown in Fig. 2(c). Fig. 9 exhibits the phase and magnitude distributions of the E-field in the air cavity of Ant 2 and Ant 3 at 25 GHz. It is obvious that the phase distribution of Ant 3 is much more consistent than that of Ant 2, and the magnitude distribution of Ant 3 close to the horn aperture is more uniform compared with that of Ant 2. The working mechanism is that the Metal-Via Array 1 equal to the mushroom structure equivalently lowers the permittivity of the region around the horn edge, which is proved by the formula (7) in [19]

$$\varepsilon_{reff} = (\varepsilon_{r1}+1)/2 + (\varepsilon_{r1}-1)/\left(2\sqrt{1+12h/W_p}\right). \quad (7)$$

The thickness of substrate 2 is h and W_p is the length of Metal-Via Array 1. According to formula (6), the phase velocity in the edge of Ant 3 speeds up [5], and the gain in low-frequency band is enhanced compared with Ant 2, which is illustrated in Fig. 8. Compared with Ant 2, the average gain of Ant 3 is increased from 9.2 to 9.9 dBi.

To prove the applicability of formula (7) further, we simulated the effect of parameter W_p on the phase distribution of the E-field. According to formula (7), the decrease of parameter W_p will decrease the permittivity ε_{reff}, which means the phase velocity v_p around the Metal-Via Array 1 will increase according to formula (6) and then the phase distribution will be more uniform. As shown in Fig. 10, the reduction of parameter W_p makes the phase distribution more uniform and the gain property becomes better. It indicates that the decrease in the length of Metal-Via Array 1 increases the phase velocity at the edge of horn antenna and lowers the permittivity of the region around the horn edge. So, a uniform phase distribution is realized, which proves the applicability of formula (7).

To further enhance the gain performance, Metal-Via Array 2 is embedded in the middle of the top and bottom substrates of the proposed antenna based on Ant 3, which is shown in Fig. 4. The top and bottom sides of substrates 1 and 3 are opened after quadratic curves are etched, and the E-field radiated from the intermediate substrate 2 is propagated in between the two metallizations of G1 and G2 (or G5 and G6). As it is depicted in Fig. 11, the E-field intensity during the top and bottom substrates of the proposed antenna is weakened, so Metal-Via Array 2 decreases the residual E-fields inside the top and bottom substrates in the high-frequency band. Therefore, the gain in the high-frequency band is improved. The average gain of the proposed antenna is enhanced from 9.9 to 10.5 dBi, compared with Ant 3, and the proposed antenna still has relatively uniform phase and magnitude distributions of E-field, which can be indicated from Fig. 12. It can be obviously seen in Fig. 8 that Metal-Via Arrays 1 and 2 improve the gain performance in the whole band. Moreover, Fig. 5(a) shows that Metal-Via Arrays 1 and 2 do not affect the impedance bandwidth of the proposed antenna much.

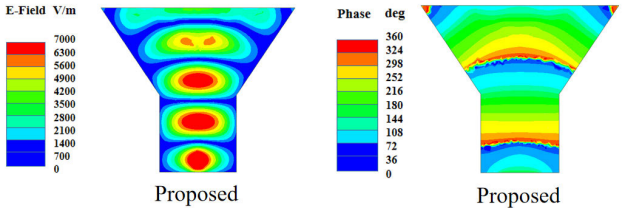

Fig. 12. Simulated E-field distributions in the air cavity of the proposed antenna at 26 GHz. (a) Magnitude. (b) Phase.

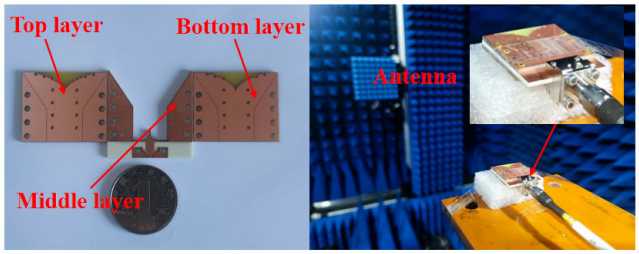

Fig. 13. Prototype of the proposed antenna and testing anechoic chamber.

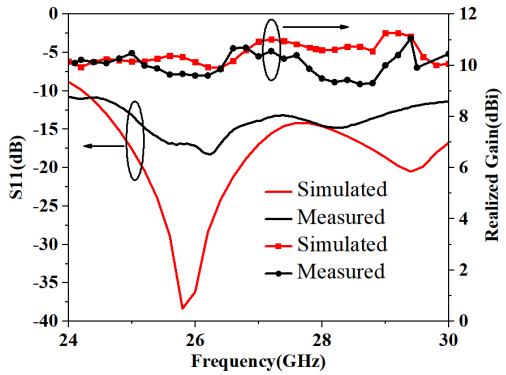

Fig. 14. Simulated and measured S11 and realized gain.

III. Measurement and Discussion

As shown in Fig. 13, the prototype of the proposed horn antenna was fabricated and tested. The reflection coefficients were measured by ZVA 40. Vector network analyzer and the radiation characteristics are obtained in the anechoic chamber. Fig. 14 exhibits the simulated and measured reflection coefficients and gains of the antenna. The measured bandwidth for $|S11| < -10$ dB is from 24 to 30 GHz, both measured and simulated operating bandwidths cover the n257, n258, and n261 5G frequency bands (24.25–29.5 GHz), and the difference between simulated and measured S-parameters may be caused by the test connector and the air gaps between substrates. From Fig. 14, it can be seen that the measured gain varies from 9.3 to 11 dBi in the operating band. Compared with the simulated gain, the measured gain decreases by approximately 1 dB from 27.8 to 29.2 GHz, which may be caused by the fabrication errors, the influence of the test connector, and the air gaps between substrates. The simulated and measured radiation patterns in the E-plane and H-plane at 26.5, 27.5, and 28.5 GHz are illustrated in Fig. 15. It is observed that the measured results are consistent with the simulated results, although the measured main lobes deviate from the endfire direction little, which may be influenced by the test connector.

For comparison with this communication, Table II illustrates the performance and structure features of the proposed horn antenna and other SIW H-plane horn antennas. From Table II, Wang et al. [6], [10] introduce two antennas that have longer longitudinal lengths to support extra gain-enhancement structures. The ESIW H-plane horn antenna in [9] has a high efficiency of around 90%, but the operating bandwidth is only 3%. The horn antenna using the slow wave structure of two substrate layers in [11] reduces the size of the antenna. Nevertheless, the gain of the antennas is around 5.5 dBi, which is low. An SIW H-horn antenna in [12] with a novel phase-corrected structure, embedded Metal-via arrays, has a maximum gain of 10.8 dBi. However, the impedance matching is not good. The horn antenna in [20] adopting the soft surface has a stable gain from 8.4 to 10.3 dBi, but its operating bandwidth is 7%. Jamshidi-Zarmehri and Neshati [21] introduce an SIW H-plane horn antenna loaded with dipole array and reflector nails, which has a high gain of 14 dBi. Nevertheless, the operating bandwidth is only 5.5%, and the reflector nails increase the overall thickness of the antenna. The SIW H-plane horn antenna in [22] realizes a high gain of 11.2 dBi with 77.6% radiation efficiency and 32.9% bandwidth by loading dielectric slab. However, it faces a challenge if directly integrated with planar circuits. Compared with the abovementioned horn antennas, the proposed H-plane horn antenna achieves a stable high-gain characteristic and the reduction of the longitudinal length of itself while obtaining the widest impedance bandwidth. In addition, the proposed antenna has the characteristics of direct integration with planar circuits.

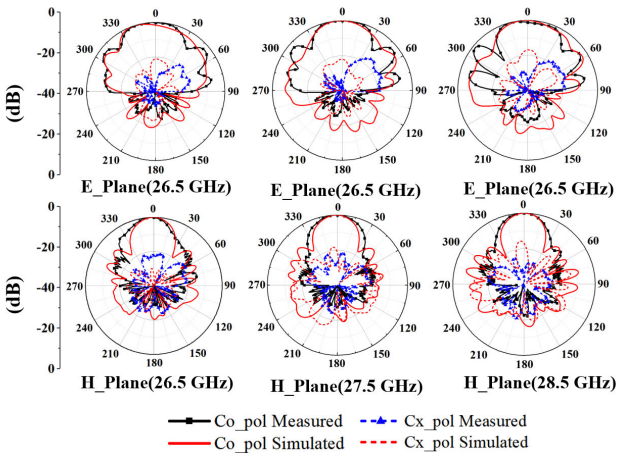

Fig. 15. Simulated and measured radiation patterns in the E-plane and H-plane at 26.5, 27.5, and 28.5 GHz.

TABLE II

Performance Comparisons Between the Proposed Antenna and Referenced H-Plane Horn Antenna

Ref	Structure	BW(%)	Gain(dBi)	Dimension ($\lambda\times\lambda\times\lambda$)
[6]	Single layer	20	10-11	2.3×**4.4**×0.17
[9]	Multi-layer	3	8.9	2.1×**5.35**×0.3
[10]	Multi-layer	15.5	10.8-12.5	4.5×**5.8**×0.32
[11]	Multi-layer	11	5.1-5.5	2.18×**2.24**×0.14
[12]	Single layer	n.g.	6-10.8	1.7×**3.2**×0.16
[20]	Multi-layer	7	8.4-10.3	2.8×**4.9**×0.2
[21]	Single layer	5.5	13-14	2.2×**1.5**×0.58
[22]	Multi-layer	32.9%	11.2	2.15×**2.98**×0.34
This work	Multi-layer	22	9.3-11	2.3×**2.9**×0.42

IV. Conclusion

This communication introduces a miniaturized ESIW H-plane horn antenna in the form of three substrates. The quadratic curves etched on the metal layers of top and bottom substrates improve the impedance matching between the radiating aperture and air. The phase-corrected structure composed of the quadratic curves embedded metal-via arrays enhances the gain performance and reduces the antenna's dimension. According to the measured results, the proposed horn antenna has a wide bandwidth of 21% and achieves a stable gain from 9.3 to 11 dBi during the operating band. In addition, the transition from microstrip line to ESIW makes the proposed antenna, which can be integrated with planar circuits. With the advantages of a wide bandwidth, stable gain performance, and ease of fabrication with low cost, this design can be applied as the feed antenna and signal antenna in future 5G wideband mmW wireless communication.

References

[1] W. Hong et al., "The role of millimeter-wave technologies in 5G/6G wireless communications," *IEEE J. Microw.*, vol. 1, no. 1, pp. 101–122, Jan. 2021.

[2] J. Deng et al., "Horn antenna with miniaturized size and increased gain by loading slow wave periodic metal blocks," *IEEE Trans. Antennas Propag.*, vol. 69, no. 4, pp. 2365–2369, Apr. 2021.

[3] Z. Li, X.-P. Chen, and K. Wu, "A surface mountable pyramidal horn antenna and transition to substrate integrated waveguide," in *Proc. Int. Symp. Signals, Syst. Electron. (ISSSE)*, Aug. 2007, pp. 607–610.

[4] Z. Li, K. Wu, and T. A. Denidni, "A new approach to integrated horn antenna," in *Proc. 10th Int. Symp. Antenna Technol. Appl. Electromagn. URSI Conf. (ANTEM)*, Jul. 2004, pp. 1–3.

[5] M. Esquius-Morote, B. Fuchs, J.-F. Zürcher, and J. R. Mosig, "A printed transition for matching improvement of SIW horn antennas," *IEEE Trans. Antennas Propag.*, vol. 61, no. 4, pp. 1923–1930, Apr. 2013.

[6] L. Wang, M. Esquius-Morote, H. Qi, X. Yin, and J. R. Mosig, "Phase corrected H-plane horn antenna in gap SIW technology," *IEEE Trans. Antennas Propag.*, vol. 65, no. 1, pp. 347–353, Jan. 2017.

[7] Y. Cai et al., "Compact wideband SIW horn antenna fed by elevated-CPW structure," *IEEE Trans. Antennas Propag.*, vol. 63, no. 10, pp. 4551–4557, Oct. 2015.

[8] A. Belenguer, H. Esteban, and V. E. Boria, "Novel empty substrate integrated waveguide for high-performance microwave integrated circuits," *IEEE Trans. Microw. Theory Techn.*, vol. 62, no. 4, pp. 832–839, Apr. 2014.

[9] J. Mateo, A. M. Torres, A. Belenguer, and A. L. Borja, "Highly efficient and well-matched empty substrate integrated waveguide H-plane horn antenna," *IEEE Antennas Wireless Propag. Lett.*, vol. 15, pp. 1510–1513, 2016.

[10] J. Wang, F. Wu, Z. H. Jiang, Y. Li, and D. Jiang, "A millimeter-wave substrate integrated waveguide H-plane horn antenna with enhanced gain and efficiency," *IEEE Antennas Wireless Propag. Lett.*, vol. 21, no. 4, pp. 769–773, Apr. 2022.

[11] Y. Zhang, J. Deng, D. Sun, J. Yin, and L. Guo, "Compact slow-wave SIW H-plane horn antenna with increased gain for vehicular millimeter wave communication," *IEEE Trans. Veh. Technol.*, vol. 70, no. 7, pp. 7289–7293, Jul. 2021.

[12] L. Wang, X. Yin, S. Li, H. Zhao, L. Liu, and M. Zhang, "Phase corrected substrate integrated waveguide H-plane horn antenna with embedded metal-via arrays," *IEEE Trans. Antennas Propag.*, vol. 62, no. 4, pp. 1854–1861, Apr. 2014.

[13] J. Wang et al., "Wideband dipole array loaded substrate integrated H-plane horn antenna for millimeter waves," *IEEE Trans. Antennas Propag.*, vol. 65, no. 10, pp. 5211–5219, Oct. 2017.

[14] Y. Cai, Z.-P. Qian, Y.-S. Zhang, J. Jin, and W.-Q. Cao, "Bandwidth enhancement of SIW horn antenna loaded with air-via perforated dielectric slab," *IEEE Antennas Wireless Propag. Lett.*, vol. 13, pp. 571–574, 2014.

[15] Y. Luo and J. Bornemann, "Substrate integrated waveguide horn antenna on thin substrate with back-lobe suppression and its application to arrays," *IEEE Antennas Wireless Propag. Lett.*, vol. 16, pp. 2622–2625, 2017.

[16] K. Iigusa, K. Li, K. Sato, and H. Harada, "Gain enhancement of H-plane sectoral post-wall horn antenna by connecting tapered slots for millimeter-wave communication," *IEEE Trans. Antennas Propag.*, vol. 60, no. 12, pp. 5548–5556, Dec. 2012.

[17] Y. Pan, Y. Cheng, and Y. Dong, "Dual-polarized directive ultrawideband antenna integrated with horn and Vivaldi array," *IEEE Antennas Wireless Propag. Lett.*, vol. 20, no. 1, pp. 48–52, Jan. 2021.

[18] Y. Zhao, Z. Shen, and W. Wu, "Conformal SIW H-plane horn antenna on a conducting cylinder," *IEEE Antennas Wireless Propag. Lett.*, vol. 14, pp. 1271–1274, 2015.

[19] W. Liu, Z. N. Chen, and X. Qing, "Metamaterial-based low-profile broadband mushroom antenna," *IEEE Trans. Antennas Propag.*, vol. 62, no. 3, pp. 1165–1172, Mar. 2014.

[20] N. Bayat-Makou and A. A. Kishk, "Substrate integrated horn antenna with uniform aperture distribution," *IEEE Trans. Antennas Propag.*, vol. 65, no. 2, pp. 514–520, Feb. 2017.

[21] H. Jamshidi-Zarmehri and M. H. Neshati, "Design and development of high-gain SIW H-plane horn antenna loaded with waveguide, dipole array, and reflector nails using thin substrate," *IEEE Trans. Antennas Propag.*, vol. 67, no. 4, pp. 2813–2818, Apr. 2019.

[22] Z. Qi, X. Li, J. Xiao, and H. Zhu, "Dielectric-slab-loaded hollow substrate-integrated waveguide H-plane horn antenna array at Ka-band," *IEEE Antennas Wireless Propag. Lett.*, vol. 18, no. 9, pp. 1751–1755, Sep. 2019.